Source rupture process of the 2011 Tohoku-Oki earthquake derived from the strong-motion records

W. Suzuki & S. Aoi
National Research Institute for Earth Science and Disaster Prevention, Japan

H. Sekiguchi
Disaster Prevention Research Institute, Kyoto University, Japan

T. Kunugi
National Research Institute for Earth Science and Disaster Prevention, Japan

SUMMARY:
We reveal the source rupture process using the strong-motion data by the inversion analysis. The derived slip distribution shows one prominently large slip area extending from the hypocentre area to the shallow part of the fault along the trench axis, which is located far off the coastal region extensively damaged by the tsunamis. The shallow main rupture started 60 seconds after the initial break and lasted for as long as 40 seconds. The deeper area between the hypocentre and the coastline experienced the two down-dip ruptures at 20-50 and 70-100 seconds. Distinctive phase observed in the low-frequency velocity waveforms is generated by the rupture of these two areas after 60 seconds. Rupture after 100 seconds propagated southward. Our result suggests that the large extent of the rupture area resulted in large ground motions across wide regions and the shallow large slip triggered the devastating tsunamis.

Keywords: Tohoku-Oki earthquake, source rupture process, strong motions, waveform inversion

1. INTRODUCTION

On March 11, 2011, the largest earthquake ever recorded in and around Japan occurred off the Pacific coast of Tohoku district, northeast Japan. The moment magnitude (M_W) of this Tohoku-Oki earthquake determined by various institutes ranges from 9.0 (e.g., Japan Meteorological Agency) to 9.1 (e.g., Global CMT project). Offshore of northeast Japan, the Pacific plate moves westward at a speed of approximately 8 cm/year and subducts from the Japan Trench beneath the Eurasian plate, on which Japanese islands are situated. The hypocentre distribution and focal mechanisms indicate that the Tohoku-Oki earthquake initiated far off Miyagi prefecture and ruptured a 400- or 500-km-long plate boundary between these two plates. This huge earthquake caused tremendous damage to eastern Japan, resulting in approximately 20,000 people killed or missing, due to the devastating tsunamis and the severe ground shaking. Maximum tsunami heights of greater than 20 m and 10 m are distributed along 290 km and 425 km of coast, respectively (Mori *et al*., 2011). These tsunamis were the primary cause of the catastrophic disaster accompanied by the earthquake. The strong ground motions with large acceleration and a long duration also caused heavy damages over wide area from Tohoku to Kanto districts, while the percentage of the human and property loss is smaller than tsunamis. It is necessary to reveal how the fault ruptured during the damaging earthquakes for understanding the generation mechanisms of the strong motions and tsunamis, and then anticipating the future earthquakes to mitigate the disasters accompanied by them. Strong-motion data, which are observed at close distances from the source fault, provide the detail information about rupture process. National Research Institute for Earth Science and Disaster Prevention (NIED) has maintained nation-wide strong-motion networks in Japan and studied the source rupture process of the large earthquakes using the strong-motion data observed by these networks. Facing the catastrophic Tohoku-Oki earthquake, we first presented the preliminary rupture model in two days (NIED, 2011) and continued to update it (Suzuki *et al*., 2011). In the present paper, we present the source rupture process derived from the strong-motion records and discuss the generation of the strong motions and tsunamis.

2. STRONG-MOTION CHARACTERISTICS OF THE 2011 TOHOKU-OKI EARTHQUAKE

Figure 2.1 shows the distribution of the peak ground acceleration (PGA) and the record section of the strong-motion waveforms observed at K-NET and KiK-net (Aoi *et al*., 2011) stations maintained by the NIED. The PGAs are calculated by the vector summation of the three components. It can be seen that the large accelerations larger than 500 gal are distributed over the area extending as long as nearly 400 km along the Pacific coast side of northeastern Japan. In the acceleration waveforms, there are two distinct wave groups (referred to as groups 1 and 2 in Figure 2.1) that arrive first at stations in Miyagi prefecture and then at northern and southern stations, almost uniformly separated by approximately 40 seconds. This observation suggests that two rupture events that radiated the seismic wave with the large accelerations occurred off Miyagi prefecture. Another distinct wave group propagates from Fukushima prefecture (group 3), just after group 2, and brings the maximum amplitude to the southern stations. This implies the possibility of the southern rupture event. Thus, the record section of the observed acceleration waveforms itself appears to provide an image of the source rupture process, which seems to consist of the several rupture events. The seismic waves radiated from these rupture events contributes to the very long durations of strong shaking across wide area. The traces of these notable acceleration wave groups, however, do not exactly correspond to the distinctive phases observed in the low-frequency (0.01-0.05 Hz) velocity waveforms. For example, although velocity waveforms have two phases for Miyagi prefecture, the amplitudes of these two phases are not comparable unlike acceleration waveforms and the latter one with larger amplitude has a peak between groups 1 and 2. The acceleration record section shows only one aspect of the entire rupture of this huge earthquake, which is considered to have frequency-dependent characteristics (e.g., Ide *et al*., 2011). We focus on the rupture process from the lower-frequency waveforms in the present paper.

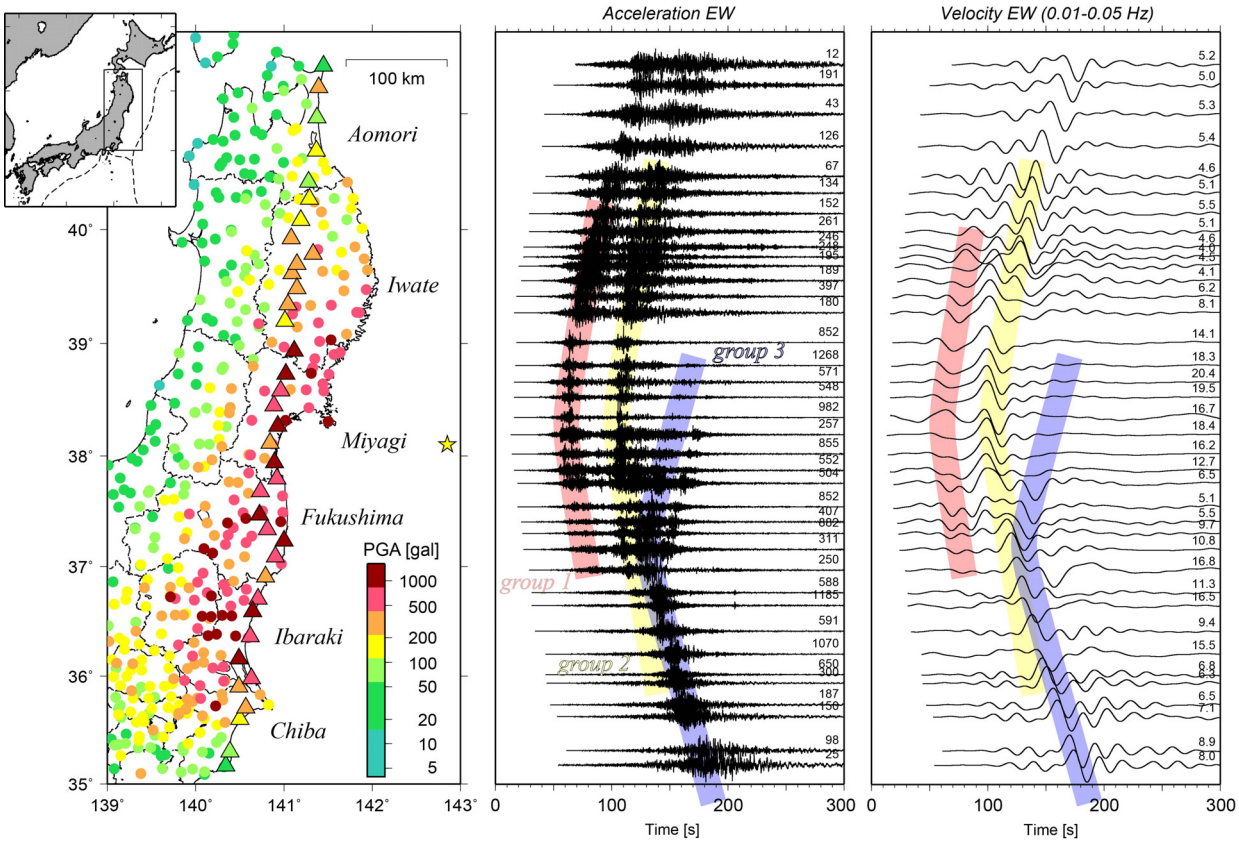

Figure 2.1. (Left) Distribution of the peak ground acceleration (PGA) recorded by K-NET and KiK-net. A star indicates the epicentre. Record section of EW-component waveforms observed at stations indicated by triangle in the left panel aligned in latitude for (middle) the non-filtered acceleration and (right) velocity bandpass filtered between 0.01 and 0.05 Hz. These traces are normalized by the maximum values denoted in the upper right of each trace. Color curves indicate the significant wave groups observed in the acceleration record section.

3. WAVEFORM INVERSION ANALYSIS

3.1. Methodology

Seismic waves radiated from the earthquake source can be modelled by integrating the response to a unit slip (Green's function) convolved with the slip velocity over the entire fault. If the sufficient data set of waveforms and well-approximated Green's functions are available, the source rupture process or the spatio-temporal slip distribution on the fault can be derived by solving inverse problem. In the present study, we use the multi-time-window linear waveform inversion method (e.g., Olson and Apsel, 1982; Hartzell and Heaton, 1983). In this method, the fault plane is discretized into subfaults and the slip history of each subfault is discretized using basis functions (time windows). Thus, the slip of time window is linearly related to the observed waveforms, and therefore, we can take advantage of least squares algorithm using the multi-time-window technique.

3.2. Fault model

We construct the rectangular fault model as shown in Figure 3.1, which has the strike angle of 195°, the dip angle of 13°, and the hypocentre depth of 24 km determined by the Japan Meteorological Agency. This fault model approximates the upper boundary of the subducting Pacific plate (Hasegawa *et al*., 1994) very well, particularly around the hypocentre. The fault length along the strike direction and width along the dip direction are set to 500 km and 200 km, respectively, so that the projection of the fault model covers the epicentres of the aftershocks. The depths of the top and bottom edges of the fault plane are 8.3 km and 53.2 km, respectively. Two large aftershocks (M_W > 7) that have the thrust-type mechanisms occurred near the northern and southern edges of the fault area.

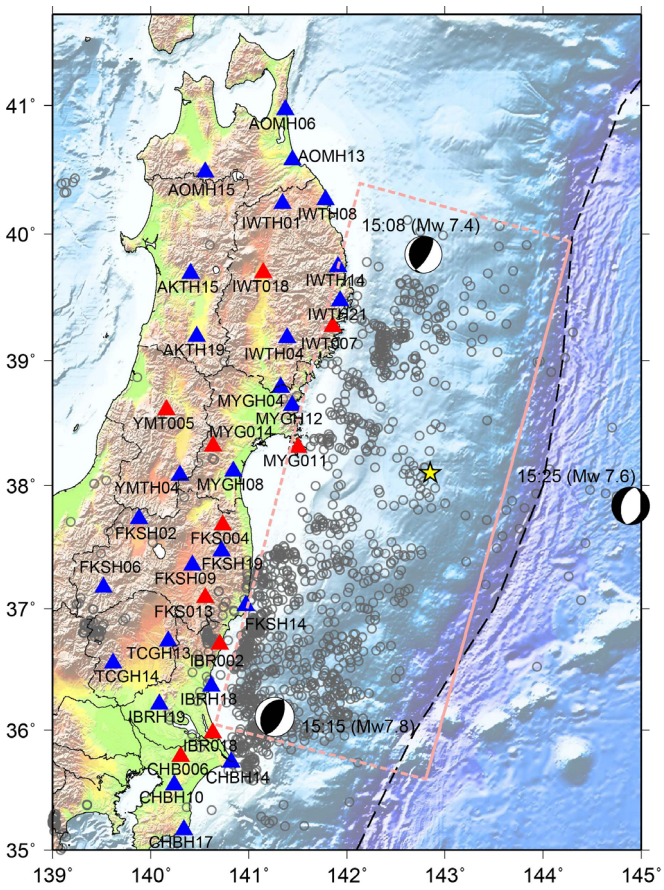

Figure 3.1. Fault model (pink rectangle) and strong-motion stations (▲: K-NET, ▲: KiK-net) used in the inversion analysis. A star and grey circles indicate the epicentres of the mainshock and earthquakes that occurred in 24 hours after the mainshock, respectively.

3.3. Strong-motion data

Considering the spatial distribution (approximately 50 km interval) and the quality of the records in the low-frequency range, 10 K-NET and 26 KiK-net stations are selected in the present study (Figure 3.1). The distances from the epicentre to the stations range from 120 km to 400 km. These distances are smaller than the extent of the fault plane, and therefore, the waveforms recorded at these stations could be regard as near-source data. K-NET stations are deployed on the ground while KiK-net stations have a pair of seismographs in borehole (depths >= 100 m) as well as on the ground surface. We used the borehole records for KiK-net stations. Data set for the inversion analysis consists of *S*-wave portion of the velocity waveforms calculated from the 100-Hz sampling original acceleration waveforms by bandpass-filtering between 0.01-0.125 Hz (8-100 seconds in period range), integration, and resampling at 1 Hz. Duration of the strong-motion data ranges from 225 seconds to 280 seconds.

3.4. Green's function

Method to calculate the Green's functions is based on the discrete wavenumber method (Bouchon, 1981) and the reflection/transmission matrix method (Kennett and Kerry, 1979) assuming the one-dimensional layered underground structure model. The assumption of the one-dimensional underground model, though for the subduction zone, is not inappropriate because the very-low-frequency content, which is less affected by small-scale underground heterogeneity, is dominant in the frequency range used in the present analysis (Suzuki *et al*., 2011). Underground structure models are constructed by referring to the three-dimensional sedimentary and one-dimensional crustal structure models proposed by Fujiwara *et al*. (2009). We consider the rupture propagation effect inside the subfault by calculating the Green's functions at multiple point sources (9 × 9) uniformly distributed over each subfault (e.g., Wald *et al*., 1996).

3.5. Analysis conditions

Rectangular fault model is divided by a square on 20 km a side into 25 × 10 subfaults. Slip of each subfault is set to start at a triggered time defined by a circle propagating from the hypocentre with constant velocity (*Vr*). The slip-velocity time function after the triggered time is represented by 6-second time windows, each of which is separated by 3 seconds. Our previous study (Suzuki *et al*., 2011) shows that the area around the hypocentre and the shallower area far off Miyagi prefecture experienced slip events for a long time. For these areas, we set 30 time windows, which allow each subfault to slip for 93 seconds. Since this slip duration seems so long for the other areas that the inversion analysis could become less stable, we gradually decreases the number of the time windows as departing from the hypocentre area. We perform the inversion using the several values of *Vr* and choose the rupture model that minimizes the misfit. Two constraints are posed to stabilize the inverse problem. One constraint limits the variation of the slip angle within 90° centred at 90°, or pure dip-slip angle, by using the least square method with an inequality constraint (Lawson and Hanson, 1974). Second, we smoothed the model parameters in space and time simultaneously following the formulation proposed by Sekiguchi *et al*. (2000). The characteristics of the present study that differ from our previous one (Suzuki *et al*., 2011) are followings: 1) The subfault size is finer. 2) The number of the time windows is assumed more flexibly depending on subfault. 3) The method to represent the rupture propagation effect inside the subfault is different.

4. INVERSION RESULT

Figure 4.1 shows the total slip distribution projected on the map. A large slip area where the slip is larger than 20 m extends from the area around the hypocentre to the shallower part of the fault plane far off the coast of Iwate, Miyagi, and Fukushima prefectures along the Japan Trench with the amount of slip increasing. The maximum slip is 42 m observed approximately 70 km east-northeast of the hypocentre. *Vr* is 2.8 km/s and the seismic moment is 4.74×10^{22} Nm (M_w9.1). The slip directions of the shallow slip area spread radially with the largest slip at a centre. Compared to the area shallower than the hypocentre, the deeper areas have relatively smaller slip.

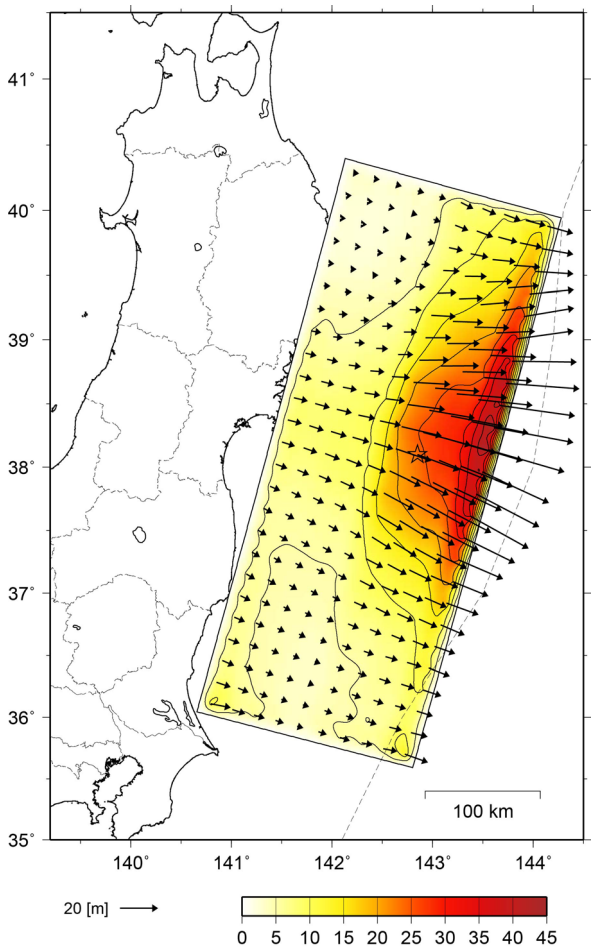

Figure 4.1. Slip distribution projected on the map. The arrows indicate the slip direction of the hanging wall side. The contour interval is 5 m. Dotted line drawn on the sea indicates the Japan Trench.

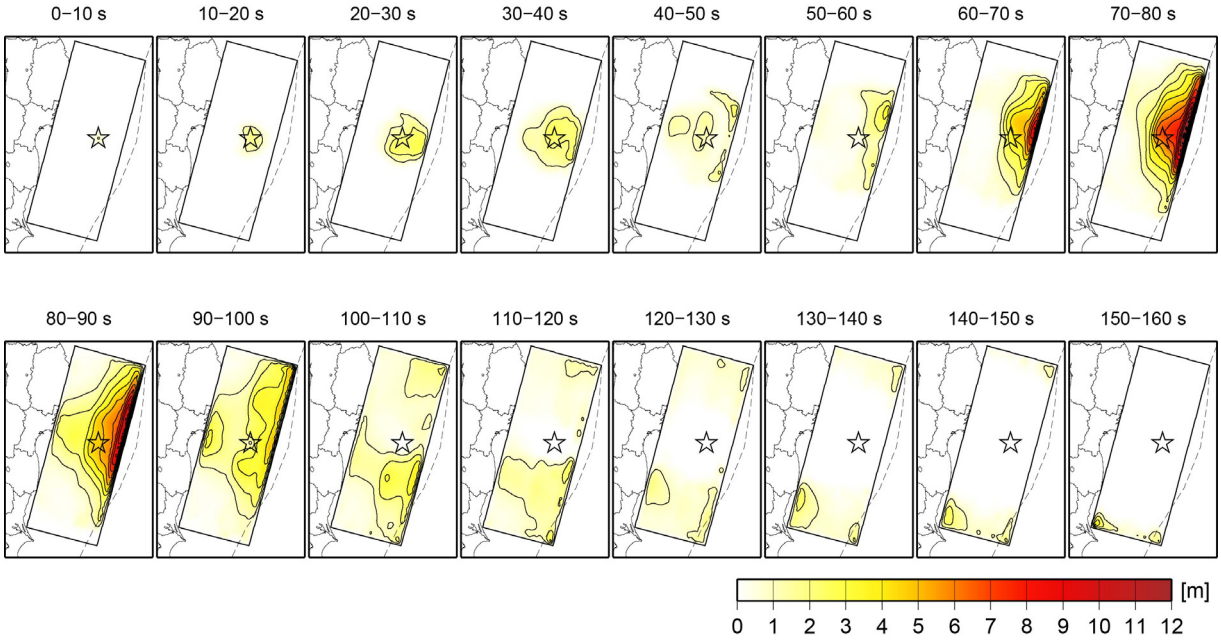

Figure 4.2. Distribution of the slip amount every 10-second time window from the initial break. The contour interval is 1 m.

Figure 4.2 shows the progression of the slip in terms of the slip distribution in every 10-second time window. The initial rupture propagated from the hypocentre and reached the shallowest part of the fault in 20-30-second time window. After 30 seconds, the shallow rupture propagated toward the northern and southern directions along the trench axis for 30 seconds. The rupture in the deeper region, off Miyagi prefecture, is also observed, which propagated in the down-dip direction, namely, toward the coastline. After 60 seconds, a larger slip occurred between the area around the hypocentre and the area along the trench axis, with the largest slip in the shallowest part. This slip propagated along the trench axis and also in the down-dip direction again after 70 seconds. The shallow slip continued for longer than 30 seconds. The deep rupture started from the area to the north of the hypocentre and reached the bottom edge of the fault in 80-90-second time window. In 80-100-second time windows, whole of off Miyagi prefecture region was ruptured from the axis line to the coastline. Rupture after 100 seconds propagated southward in the area off Fukushima and Ibaraki prefectures.

Comparison between the observed and synthetic waveforms is shown in Figure 4.3. The synthetic waveforms fit the observed ones very well.

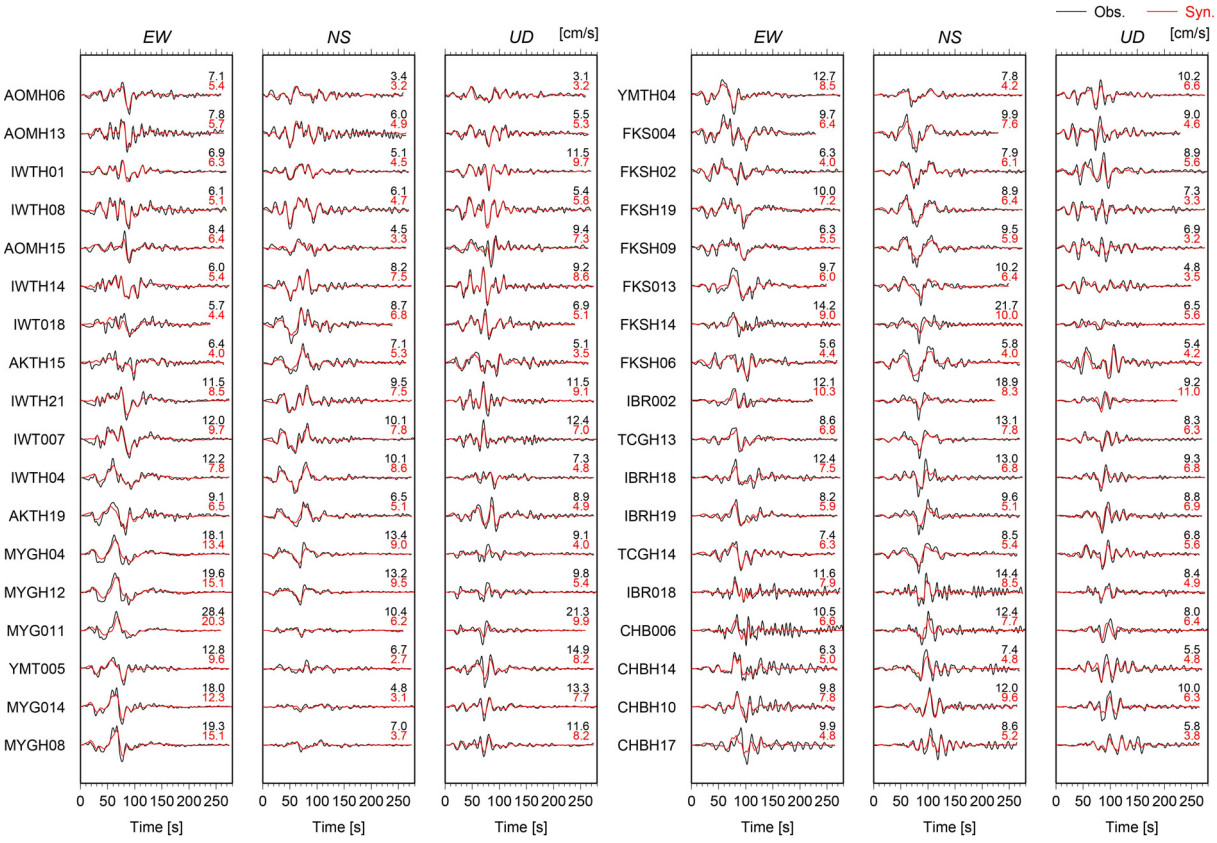

Figure 4.3. Comparison between the observed (black) and synthetic (red) waveforms. Maximum values (cm/s) are denoted in the upper right of each trace.

5. EXAMINATION OF THE RUPTURE PROCESS RELATED TO STRONG MOTION AND TSUNAMI GENERATION

The slip distribution (Figure 4.1) indicates that off Miyagi prefecture region, where the hypocentre is situated, has large slip greater than 5 m from the area near the trench axis to the coastline. Before the Tohoku-Oki earthquake, a part of off Miyagi prefecture region near the coastline was regarded as a high-risk area for earthquake of magnitude 7~8 (e.g., Earthquake Research Committee, Headquarters for Earthquake Research Promotion, 2005), however the possibility of the rupture of the whole off Miyagi prefecture region including the shallower part has not been considered. Figure 4.2 shows that

most of off Miyagi prefecture region once experienced some slips during the first 60-second rupture. After that, much larger slips occurred and expanded to the entire off Miyagi prefecture region. The synthetic waveforms generated by the 60-100-second rupture of the whole off Miyagi prefecture region are shown in Figure 5.1. It can be seen that this rupture event can reproduce the main feature of the largest phase of the low-frequency velocity waveforms at stations located between Aomori and Fukushima prefectures. It also generates the main phase observed at the southern stations to some degrees. If we divide off Miyagi prefecture region into the shallow and deep parts, the deep part, though smaller slip, reproduces the waveforms of the larger amplitude observed at Miyagi and northern Fukushima prefectures. For these stations, the shallow part seems to contribute in the low-frequency content of the main phase. Contrary, the shallow part has a larger contribution to the synthesis of the main phase at Aomori, Iwate and southern Fukushima, Ibaraki, and Chiba prefectures. Thus, the main rupture of off Miyagi prefecture region characterizes the low-frequency waveforms of the Tohoku-Oki earthquake.

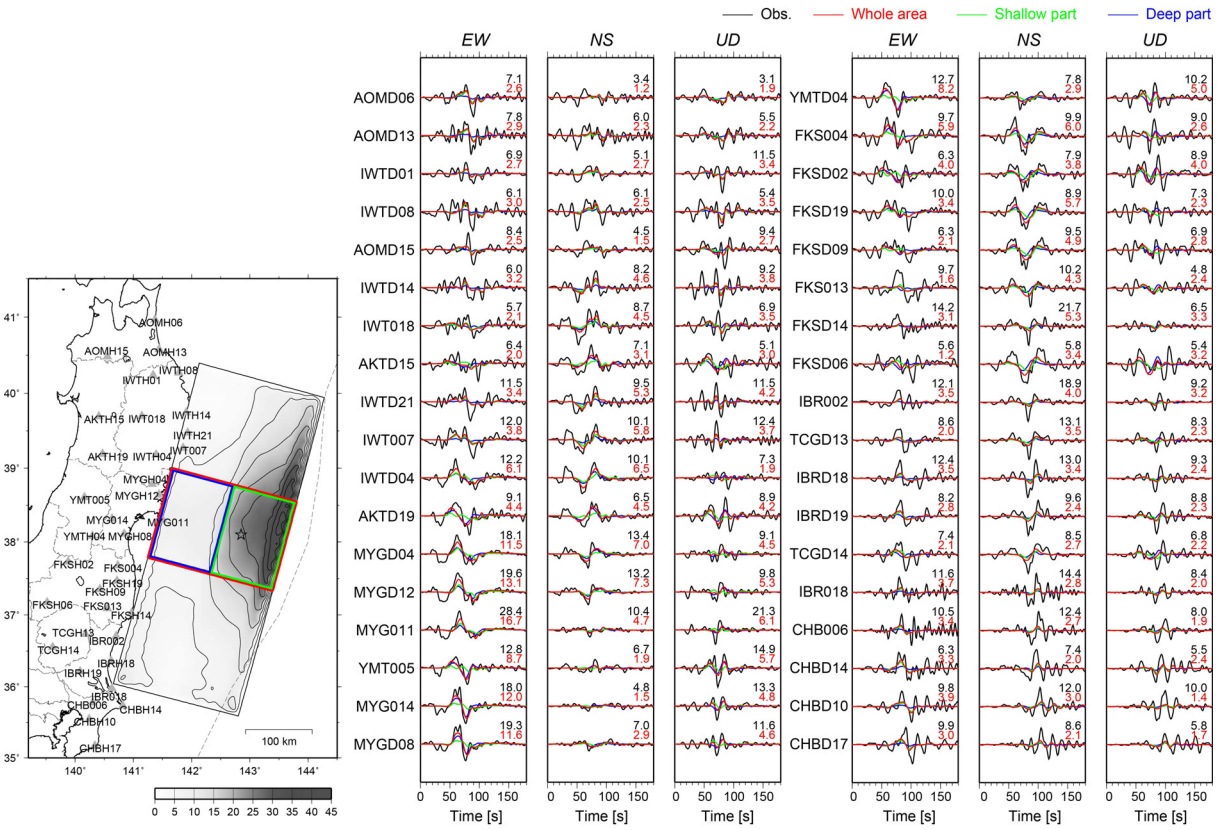

Figure 5.1. Synthetic waveforms reproduced by the ruptures of the whole off Miyagi prefecture region (red), the shallow part (green) and the deeper part (blue) of off Miyagi prefecture region, which occurred 60-100 seconds after the initial break.

Figure 2.1 suggests that the characteristics of the acceleration waveforms dominated by the high-frequency content differ from the low-frequency velocity waveforms and the main sources of the high- and low-frequency seismic waves are not necessarily the same. There are several studies of modelling the strong-motion waveforms that are higher than 0.1 Hz (e.g., Asano and Iwata, 2011; Irikura and Kurahashi, 2012; Kawabe *et al*., 2011). These studies set two sources off Miyagi prefecture region in area deeper than the hypocentre, which are responsible for the two wave groups notable in acceleration records (groups 1 and 2 in Figure 2.1). In addition, they assumed the sources in the southern source area, off Fukushima and Ibaraki prefectures, to simulate the wave group observed in the higher-frequency waveforms at southern stations (group 3). From the waveform synthesis and the *S*-wave arrival time by the distinctive rupture events, we also speculated that the two down-dip ruptures off Miyagi prefecture generated groups 1 and 2 and the rupture propagating southward is responsible for group 3 (Suzuki *et al*., 2011). The shallow large slip derived from the source inversion

analysis using the low-frequency waveforms may have little contribution to the large acceleration observed along the Pacific coast side of eastern Japan during the Tohoku-Oki earthquake. Repeated ruptures in off Miyagi prefecture region and large extent of the rupture area along strike direction are possible causes of severe ground motions with a long duration across wide region of eastern Japan.

As shown so far, our slip model has one prominent large slip area extending from the hypocentre area into the shallow part of the fault plane along the trench axis, far off the coast of southern Iwate, Miyagi, and northern Fukushima prefectures, where the tsunami damage was extensive. This large slip near the trench is consistent with the slip model estimated from the seafloor displacement (Ito *et al*., 2011). Fujii *et al*. (2011) and Maeda *et al*. (2011) derived the largest slip on the subfault nearest to the trench axis, off Miyagi prefecture, by modelling the tsunami data. Saito *et al*. (2011) also obtained the large slip area along trench axis from the inversion of the tsunami waveforms, though the maximum slip is located between the trench axis and the hypocentre. These characteristics of the slip distribution derived from the tsunami data imply that the large slip that occurred in the area between the hypocentre and the trench line found in the present study caused the devastating tsunami.

6. CONCLUSION

We derive the source rupture process of the devastating 2011 Tohoku-Oki earthquake using the low-frequency strong-motion waveforms by the multi-time-window inversion technique. In off Miyagi prefecture region, the large slip is estimated from the trench axis to the coastline with particularly large slip in the shallow part. This region experienced the two rupture events. The second rupture was larger in terms of the slip amount and the extent of the rupture area, and characterized the main phase observe in the low-frequency velocity waveforms. After the second rupture in off Miyagi prefecture region, the rupture expanded southward. The repeated rupture and the large extent of seismic sources would result in large ground motions with a long duration across wide regions. Moment magnitude calculated from the whole rupture is 9.1, which is the largest value ever recorded in Japan. The shallow large slip, which had not been anticipated before the earthquake, could trigger the devastating tsunamis.

AKCNOWLEDGEMENT
We used the hypocentre information provided by the Japan Meteorological Agency. Figures were drawn using the Generic Mapping Tools (Wessel and Smith, 1991).

REFERENCES

Aoi, S., Kunugi, T., Nakamura, H. and Fujiwara, H. (2011). Deployment of new strong-motion seismographs of K-NET and KiK-net. *Earthquake Data in Engineering Seismology*, 167-186, Springer.

Asano, K. and Iwata, T. (2011). Strong Ground Motion Generation during the 2011 off the Pacific Coast of Tohoku Earthquake Revealed by the Broadband Strong Motion Simulation. *Seismological Society of Japan, 2011 Fall Meeting*, A11-06, http://sms.dpri.kyoto-u.ac.jp/k-asano/pdf/ssj2011_a11-06.pdf (in Japanese).

Bouchon, M. (1981). A simple method to calculate Green's function for elastic layered media. *Bulletin of the Seismological Society of America* **71: 4**, 959-971.

Earthquake Research Committee, Headquarters for Earthquake Research Promotion. (2005). Report: 'National Seismic Hazard Maps for Japan (2005)', http://www.jishin.go.jp/main/chousa/06mar_yosoku-e/index-e.htm

Fujii, Y., Satake, K., Sakai, S., Shinohara, M. and Kanazawa, T. (2011). Tsunami source of the 2011 off the Pacific coast of Tohoku Earthquake. *Earth, Planets and Space* **63:7**, 815-820.

Fujiwara, H., Kawai, S., Aoi, S., Morikawa, N., Senna, S., Kudo, N., Ooi, M., Hao, K., Hayakawa, Y., Toyama, N., Matsuyama, H., Iwamoto, K., Suzuki, H. and Liu, Y. (2009). A study on Subsurface Structure Model for Deep Sedimentary Layers of Japan for Strong-motion Evaluation. *Technical Note of the NIED* **337** (in Japanese).

Hartzell, S. H. and Heaton, T. H. (1983). Inversion of strong ground motion and teleseismic waveform data for the fault rupture history of the 1979 Imperial Valley, California, earthquake. *Bulletin of the Seismological Society of America* **73: 6**, 1553-1583.

Hasegawa, A., Horiuchi, S. and Umino, N. (1994). Seismic structure of the northeastern Japan convergent margin: A synthesis. *Journal of Geophysical Research* **99: B11**, 22295-22311.

Ide, S., Baltay, A. and Beroza, G. C. (2011). Shallow Dyanamic Overshoot and Energetic Deep Rupture in the 2011 M_W 9.0 Tohoku-Oki Earthquake. *Science* **332**, 1426-1429.

Ito, Y., Tsuji, T., Osada, Y., Kido, M., Inazu, D., Hayashi, Y., Tsushima, H., Hino, R. and Fujimoto, H. (2011). Frontal wedge deformation near the source region of the 2011 Tohoku-Oki earthquake. *Geophysical Research Letters* **38**, L00G05.

Irikura, K. and Kurahashi, S. (2012). Strong Ground Motions during the 2011 Pacific Coast Off Tohoku, Japan Earthquake. *International Symposium on Engineering Lessons Learned from the Giant Earthquake*, http://www.kojiro-irikura.jp/pdf/One-year-after-the-2011-Tohoku_irikura_revised.pdf

Kawabe, K., Kamae, K., Uebayashi, H. and Harada, S. (2011). Source Modeling of the 2011 Tohoku-Chiho Taiheiyo-Oki Earthquake (Mw9.0). *Japan Geoscience Union Meeting 2011*, MIS036-P35, http://www.rri.kyoto-u.ac.jp/jishin/eq/tohoku2/JGU2011Taikai-v01.pdf (in Japanese).

Kennett, B. L. N. and Kerry, N. J. (1979). Seismic waves in a stratified half space, *Geophysical Journal of the Royal Astronomical Society* **57**, 557-583.

Lawson, C. L. and Hanson, R. J. (1974). Solving Least Squares Problems, Prentice-Hall, Inc., New Jersey.

Maeda, T., Furumura, T., Sakai, S. and Shinohara, M. (2011). Significant tsunami observed at ocean-bottom pressure gauges during the 2011 off the Pacific coast of Tohoku Earthquake. *Earth, Planets and Space* **63:7**, 803-808.

Mori, N., Takahashi, T., Yasuda, T. and Yanagisawa, H. (2011). Survey of 2011 Tohoku earthquake tsunami inudation and run-up. *Geophysical Research Letters* **38**, L00G14.

NIED. (2011). Source Process of the 2011 Off the Pacific Coast of Tohoku earthquake based on Strong Ground Motions (Preliminary). http://www.kyoshin.bosai.go.jp/kyoshin/topics/TohokuTaiheiyo_20110311/nied_kyoshin2e.pdf

Olson, A. H. and Apsel, R. J. (1982). Finite faults and inverse theory with applications to the 1979 Imperial Valley earthquake. *Bulletin of the Seismological Society of America* **72: 6**, 1969-2001.

Saito, T., Ito, Y., Inazu, D. and Hino, R. (2011). Tsunami source of the 2011 Tohoku-Oki earthquake, Japan: Inversion analysis based on dispersive tsunami simulations. *Geophysical Research Letters* **38**, L00G19.

Sekiguchi, H., Irikura, K. and Iwata, T. (2000). Fault geometry at the rupture termination of the 1995 Hyogo-ken Nanbu earthquake, *Bulletin of the Seismological Society of America* **90:1**, 117-133.

Suzuki, W., Aoi, S., Sekiguchi, H. and Kunugi, T. (2011). Rupture process of the 2011 Tohoku-Oki mega-thrust earthquake (M9.0) inverted from strong-motion data. *Geophysical Research Letters* **38**, L00G16.

Wald, D. J., Heaton, T. H. and Hudnut, K. W. (1996). The Slip History of the 1994 Northridge, California, Earthquake Determined from Strong-Motion, Teleseismic, GPS, and Leveling Data. *Bulletin of the Seismological Society of America* **86:1B**, S49-S70.

Wessel, P. and Smith, W. H. F. (1991). Free software helps map and display data. *Eos, Transactions, American Geophysical Union* **72**, 441.